Modelling endoplasmic reticulum network maintenance in a plant cell

Congping Lin[1,2], Rhiannon R. White[3], Imogen Sparkes[3], and Peter Ashwin[2]

[1]Center for Mathematical Sciences & Hubei Key Lab of Engineering Modelling and Scientific Computing, Huazhong University of Science and Technology, Wuhan, China
[2]Mathematics, Harrison Building, University of Exeter, Exeter, UK
[3]Biosciences, Geoffrey Pope Building, University of Exeter, Exeter, UK

(May 8, 2017)

Abstract

The endoplasmic reticulum (ER) in plant cells forms a highly dynamic network of complex geometry. ER network morphology and dynamics are influenced by a number of biophysical processes, including filament/tubule tension, viscous forces, Brownian diffusion and interactions with many other organelles and cytoskeletal elements. Previous studies have indicated that ER networks can be thought of as constrained minimal-length networks acted on by a variety of forces that perturb and/or remodel the network. Here, we study two specific biophysical processes involved in remodelling. One is the dynamic relaxation process involving a combination of tubule tension and viscous forces. The other is the rapid creation of cross-connection tubules by direct or indirect interactions with cytoskeletal elements. These processes are able to remodel the ER network: the first reduces network length and complexity while the second increases both. Using live cell imaging of ER network dynamics in tobacco leaf epidermal cells, we examine these processes on ER network dynamics. Away from regions of cytoplasmic streaming, we suggest that the dynamic network structure is a balance between the two processes, and we build an integrative model of the two processes for network remodelling. This model produces quantitatively similar ER networks to those observed in experiments. We use the model to explore the effect of parameter variation on statistical properties of the ER network.

INTRODUCTION

The endoplasmic reticulum (ER) is typically the largest membrane-bound organelle in eukaryotes. In plant cells it forms an interconnected network of tubules, which grow and

connect to form polygons, and flattened sheets. The network is highly complex and highly dynamic in its geometry [1, 2, 3]. Maintaining a single ER component with possible contact to a wide range of moving organelles may be critical for cell function [4, 5]. For example, ER morphology is linked to mitochondria dynamics and biogenesis [6], and chloroplast extensions (stromules) have been reported to align with ER tubules [7]. ER movement is largely driven by actin-myosin dependent processes[2, 8, 9, 10]. How the ER maintains such a connected and dynamic structure within the cytoplasm in living cell is unclear. It is therefore important that we are able to quantify morphological changes (including polygon formation) and underpin the biophysical processes which govern ER network formation.

Various quantitative studies have managed to clarify some aspects of ER network structure (including tubule dimension, branching properties, etc.) [1, 11, 12, 13, 14]. More recently, attempts have been made to understand ER morphology in terms of optimization. These have suggested that equilibrium ER morphologies minimize a system energy (e.g. elastic energy of sheet edges and surfaces) depending on concentration of curvature-stabilizing proteins [15, 16]. In addition, persistent or static elements of the ER network have been pulled out [2, 4, 17, 18] and these persistent elements may have important roles in anchoring the network to the plasma membrane [19, 20, 21, 22]. Thus the ER is likely a constrained minimization of the network attached to these points.

In a previous paper [23] we quantified some properties of instantaneous ER networks in tobacco leaf epidermal cells. Because the ER in these cells lies within a thin layer of cytoplasm between plasma membrane and vacuole, the network of ER tubule has been approximated as a planar graph that connects persistent points which may be embedded within the plasma membrane. The ER network includes a number of cycles (polygons) that give multiple paths between points on the network, but in other ways resembles a "Steiner tree"[24] (a minimal-length tree that joins a fixed configuration of "persistent points" but where junction points/"non-persistent points" that are "Steiner points" may be added). In particular, live cell imaging data has suggested that angles at junction points are approximately 120^o while the angles at persistent points are on average larger than 120^o. We have proposed that the observed ER tubular networks can be thought of as perturbed Euclidean Steiner Networks (*ESNs*) between persistent points [23].

Briefly, an ESN is a network joining a number of persistent points that is a local minimum in length, even if additional junction points are added. Moreover, the topology of an ESN need not to be minimal: it does not need to be a tree, but can include loops. For an ESN, the angles at junction points are 120^o while angles at persistent points are larger. If either of these conditions are violated then there is a perturbation of the junction points or with an addition of junction point that reduces network length. Considering only Brownian forces, we were able in [23] to model the fluctuations of ER junction points for cells treated with Latrunculin B (LatB), which depolymerises actin. In such cells we assume only Brownian, viscous drag and ER tubule tension forces are present. However, in the native cell, not only Brownian forces but many other active motor-cytoskeletal forces are present as well as whole scale motion (streaming) in parts of the cytoplasm.

This paper uses live-cell imaging data of ER networks within the cytoplasm of individual

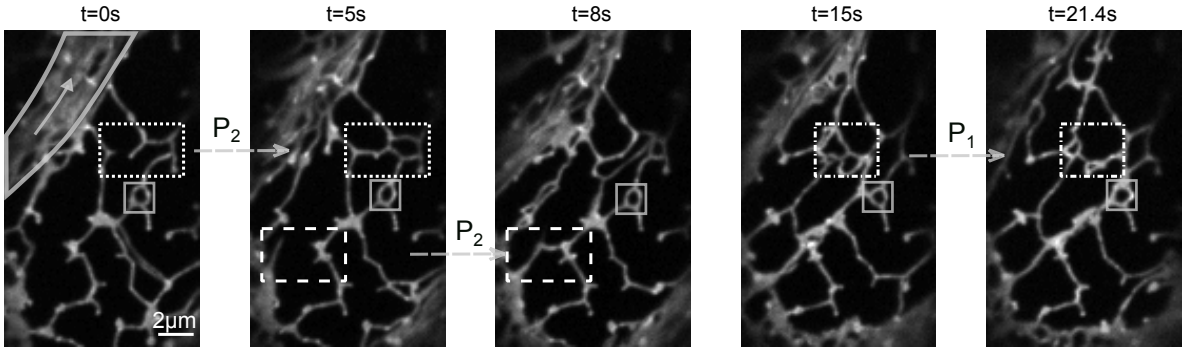

Figure 1: Some frames of a movie showing ER structural dynamics within the thin flat layer of cytoplasm between plasma membrane and vacuole for a single tobacco leaf epidermal cell in native state. The light areas indicate the location of a fluorescent marker within the ER lumen: dynamic ER tubules can be seen. Paired boxes between neighbouring frames illustrate two of the processes occurring during network dynamics: "relaxation" (P1) and "cross-connection" (P2). The solid grey arrow (in the first frame) indicates a region of ER streaming that is present throughout the movie. The ER within the small grey box remains unchanged in shape during the movie, probably due to surrounding a stationary organelle. See Movie S1 in the Supporting Material for the full movie.

tobacco leaf epidermal cells at a higher temporal resolution than [23] and so is able to identify and quantify some of the processes involved in the dynamic maintenance of this network. Because the cytoplasm is very thin, the network is effectively two dimensional and constrained to remain in the focal plane of the microscope. Using spinning disc microscopy we are able to observe and quantify (P1) "relaxation" processes of the network by ER tubule tension-driven rearrangements of the network and (P2) "cross-connection" processes where new tubules are rapidly drawn out to make links across the network. Fig. 1 (and Movie S1) illustrates an example of ER network dynamics showing these two processes at play as well as a region of streaming in the top left that we do not attempt to model in this paper. Based on integrating P1 and P2, we develop a dynamic model of ER networks between persistent points that seems to be valid away from areas of streaming. In particular there is a balance between P2 that creates an extensive network and P1 that reduces its length towards a local minimum, i.e. an ESN.

MATERIAL AND METHODS

Plant cell microscopy

Plant material and sample generation. *Nicotiana tabacum* (tobacco) plants were grown and transiently transformed using Agrobacterium infiltration methods as described in [25]. Competent, transformed Agrobacteria containing either mCherry or GFP-fusion

(HDEL) ER luminal marker constructs (ER-rk or ER-gk, [26]) were infiltrated into leaf tissue at an optical density of 0.05. Leaf samples (approximately $5mm^2$) were taken for immediate analysis from plants following 2 days of expression.

Spinning disc confocal imaging. Spinning disc confocal imaging of ER in live tobacco epidermal pavement cells was performed using a VisiScope Confocal Cell Explorer under the control of VisiView software (Visitron Systems, GmbH Germany), composed of an IX81 motorized inverted microscope (Olympus, Germany), a CSU-X1 Spinning Disc unit (Yokogawa, Japan), a PlanApo UPlanSApo 100 (1.4 NA) oil objective (Olympus, Germany) with a Photometrics CoolSNAP HQ2 camera (Roper Scientific, Germany). To achieve fluorescent imaging, GFP was excited with a Sapphire $488nm$ $70mW$ laser and mCherry with a Cobolt Jive $561nm$ $70mW$ laser. All movies were taken using a temporal resolution of $200ms$/frame, with a spatial resolution of $0.129\mu m$/pixel.

Image processing and analysis

Extraction of polygons wrapped by ER networks. Regions within a series of consecutive frames from each ER movie are selected to quantify polygons wrapped by ER. Each image is then binarized by a global thresholding (any pixel intensity smaller than a global threshold is set to 0) proportional to the median intensity of pixels in the image and a local thresholding proportional to the local maximal intensity of the neighboring 5×5 pixels. Global and local thresholds are chosen manually for each ER movie. The area (in terms of total number of pixels or μm^2) of each polygons is calculated and polygons are recorded for analysis. Polygons of area less than 20 pixels are excluded as they are strongly affected by noise. Manual correction of polygon identification is performed when necessary.

Extraction of ER networks. The region and series of consecutive frames from each ER movie are selected in order to quantify the velocity of the ER junction point and the ER tension applied on the junction point. Persistent points (and thus the number of persistent points) within the region are extracted using the method described in [23]. Positions of junction points as well as the linkages (edges) within ER networks are extracted manually.

Quantification of "cross-connection" rates. Cross-connections are quantified by counting the number of events (away from streaming) where there is creation of new tubules that link existing one together, within a regions of 50×50 pixels from each movie of $15s$ duration.

Euclidean Steiner networks Recall that a Euclidean Steiner network (ESN), as introduced in [23], is a generalization of the notion of Steiner tree (ST). Given a set of fixed points (terminals) $u_1, u_2, \cdots, u_p$ on the plane, the total length of a graph that joins these points may usually be reduced by adding extra junction points, say $x_1, x_2, \cdots, x_M$ on the plane and incorporating these into the graph. Trees whose total length is a local minimum to perturbations of the x_i or splitting of nodes are called STs [24]. However, there may be graphs that are not trees but are still local minima in length: these are ESNs. In contrast to a ST, an ESN may have non-trivial cycles but still Steiner points have degree three and vertex angles exactly 120^o. Terminals of an ESN have degree one or two (exceptionally three) and vertex angles that must be at least 120^o. Note that for a given finite set of terminals

there may be (finitely) many ESNs with differing topologies. Clearly there will be ESNs of minimal and maximal length - a minimal length network corresponds to the usual notion of minimal ST [24].

Modelling ER network dynamics

Biophysical modelling for the movement of ER junctions. The movement of ER junction points is modelled as a balance between ER surface tension force, Stokes drag force and Brownian forces using the simple biophysical model described in [23]. More specifically, the location $x(t) \in \mathbb{R}^2$ of a junction point surrounded by three persistent points moves according to the stochastic differential equation

$$6\pi\eta r\frac{dx}{dt} + F\nabla_x f(x) + \sqrt{12k_BT\pi\eta r}\xi(t) = 0 \tag{1}$$

where $F := 2\pi r\gamma$ give the tension force of a filement of radius r with surface tension γ, $f(x) := \sum_{i=1}^{3}|x-p_i|$ is the total edge length of the straight edges linking the corresponding junction point at position x to three fixed nodes at positions p_i, $i = 1, 2, 3$, k_B is the Boltzmann constant, T is temperature and $\xi(t)$ is white noise with zero mean and autocorrelation $\langle\xi(t)\xi(t')\rangle = \delta(t-t')$. Note that we assume that the tubules connecting the junction points are straight as in [23], though in reality we see a small amount of curvature in tubules that join rapidly moving points, presumably due to being dragged through stationary cytoplasm. Rearranging Eq. 1 gives

$$\frac{dx}{dt} = -b\nabla_x f(x) + \sqrt{2\sigma}\xi(t) \tag{2}$$

where $b = \frac{F}{6\pi\eta r}$ gives the effective drift coefficient and $\sigma = \frac{k_BT}{6\pi\eta r}$ the diffusion coefficient. By analysing the mean square displacement [27] of Brownian fluctuations of junction points, we estimate a diffusion rate $\sigma \approx 0.002\mu m^2\, s^{-1}$ (see Supporting Material and Fig. S1), which in a similar order to that estimated in [23] for LatB treated cells (where $\sigma \approx 0.008\mu m^2\, s^{-1}$). If we ignore Brownian fluctuations, then Eq. 2 becomes

$$\frac{dx}{dt} = b\Gamma \tag{3}$$

where $\Gamma := -\nabla_x f(x) = -\sum_i r_i/|r_i|$ is the resultant *geometric force* over directions $r_i = x - p_i \in \mathbb{R}^2$ of tubules that connect to x: when multiplied by b this gives the resultant velocity at the junction point.

Integrative modelling of ER network dynamics. We introduce a model of ER network dynamics that captures important aspects of remodelling away from regions of streaming, based on integrating the "relaxation" processes P1 and "cross-connection" process P2, between a set of persistent points. The addition of cross connection extends the biophysical model from [23]. The persistent points in the model are either (a) extracted from a specified experimental ER movie, or (b) uniformly randomly generated with the estimated number of persistent points per unit area from experimental ER movies. We ignore Brownian fluctuations so that the junction points evolve according to Eq. 3 with an effective drift

velocity b for the "relaxation" process P1: the only forces acting are the tubule tension and viscous drag. The "cross-connection" process P2 is included as a Poisson process with rate α where links are added instantaneously and at random locations. As the junction points move they can merge or draw new junction points from persistent points. This dynamically changes the geometry, and indeed the topology, of the ER network. Movie S2 shows an example of simulated network dynamics. More details of the implementation are discussed in the Supporting Material and Fig. S2.

RESULTS

Quantifying network geometry

As noted in [23], ER networks form cycles (that we refer to as polygons) between persistent points and junction points (non-persistent points). Using the image processing method described within Methods we extract persistent points and polygons from the ER images. We characterise the complex topology of the ER network by first looking at the distribution of persistent points and then exploring the distribution of polygon shape and area between persistent points.

The distance to n-th order nearest neighbours [28] is used to characterise the distribution of persistent points: Fig. 2 supports the hypothesis that persistent points are uniformly distributed in space and any apparent clustering is fortuitous. From the experiments we take regions of $13\mu m \times 13\mu m$ in $30s$-duration movies of ER within single cells, and measured on average that there are 0.27 ± 0.02 ($n = 14$) persistent points per μm^2.

The area as well as the minor and major axis length of each extracted polygon is used to explore the distribution of polygon shapes and how elongated the polygons are. The ratio (of minor to major axis length) distribution for extracted polygons within experimental observed ER networks is shown in Fig. 3(a). Note that this ratio is typically between $\frac{1}{2}$ and 1, indicating that the polygons are in general fairly rounded. Moreover, note that larger polygons are typically more round among observed polygons. Fig. 3(b) demonstrates that the polygon area is roughly half of the square of the major axis length of polygons, consistent with the polygons being rounded in shape.

The number, area and shape of polygons changes dynamically during each movie. Away from regions of streaming, we observed that the loss of polygons is mainly due to the "relaxation" process (P1) while the gain of polygons is mainly due to the "cross-connection" process (P2). We now quantify these processes in more detail in the following.

Quantifying and biophysical modelling of the relaxation process

Dynamics of ER junction points in the living cell results in remodelling of the network between a number of different topologies that seem to be close to ESNs. Indeed, we observe the ER network topology changes between different ESNs and a typical example is shown in Fig. 4(a). Note that ER tubules are approximately straight [23]. Although the tension

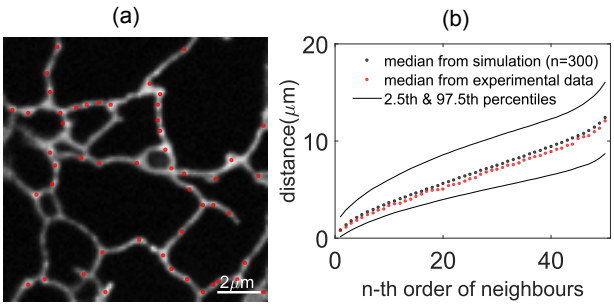

Figure 2: (a) Persistent point distribution in a space of $13\mu m \times 13\mu m$ of ER (51 persistent points in total) is displaced on one frame of an experimental ER movie (see Movie S3 in the Supporting Material); the red dots give the identified persistent points. (b) Red dots show median distance of a persistent point to its nth nearest neighbour from a number of extracted persistent points from the movie. Black dots and lines show similarly the median and extremes of the distances respectively, from 300 simulations of a uniform distribution in the same region with the same number of points.

force may depend on the concentration of particular proteins in the membrane[16], the three-way ER junctions are well described as Steiner points, suggesting constant tension between filaments [23]. Thus we simply assume here a constant tension force as in [23] and model the movement of ER junction points as in Eq. 2.

Ignoring Brownian fluctuations, the movement of junction point is governed by the effective drift coefficient b and the three-way resultant geometric force Γ, as indicated from Eq. 3. A symmetric three-way junction has $\Gamma = 0$: the junction point sits at a Steiner point giving a local minimal network. Larger values of $|\Gamma|$ correspond to more asymmetry at the junction point and faster movement of that junction point. To further test this biophysical model for the movement of junction point, we measure instantaneous values of Γ and the velocity v of the junction point during the network dynamics including moments with fast motion of junction points. Fig. 4(b) shows that the velocity and tension force are well correlated (Pearson correlation test, $p < 0.0001$) for both horizontal and vertical orientations. Moreover, the best fitting line gives the slopes $b = 1.60$ and $b = 1.15$ for the horizontal and vertical components respectively and F test suggests that there is no significant difference (p=0.109) in the best fitting slope between vertical and horizontal components. These suggest the Eq. 3 with constant drift coefficient b well models the movement of junction points. We remark here that this estimated effective drift coefficient $b \approx 1\mu m\, s^{-1}$ is of similar order to that estimated drift coefficient $0.2\mu m\, s^{-1}$ in [23] by considering the Brownian-driven fluctuations of junction points in LatB treated cells.

The geometric force Γ acts to reduce network length. It may also lead to collisions of junctions and reduction in the number of polygons through a process of *polygon collapse*, where all junction points on the boundary of a polygon meet at one or two points. Fig. 5 shows some examples of polygon collapse during the ER remodelling, and the details of collapse of one polygon. As each junction point has three edges linking to other points, it

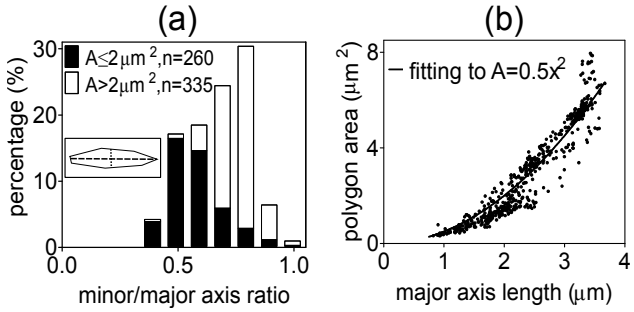

Figure 3: (a) Distribution of minor/major axis ratio for instantaneous polygons from ER movies, grouped according to polygon area. The inset shows the major (dashed line) and minor (dotted line) axes of a polygon. Observe that smaller polygons are typically more asymmetric than larger ones. (b) Polygon area A plotted against major axis length x length for the polygons from (a). The curved line shows that the relationship fits well to a quadratic function $A = ax^2$ with $a = 0.5$.

will be on the boundary of at most three polygons and so the movement of the junction point may also enlarge areas of some other polygons. The geometric force Γ will create new junction points if the motion results in an angle between tubules that is less than 120^o at a persistent point. In a special case of an ER network that is an ESN, the geometric forces on junction points are all zero and the network is stationary.

Fig. 6(a) shows the dynamics of polygon area during examples of collapse. This data suggests that polygons collapse at an approximately similar linear rate, independent of initial area and shape, and polygons collapse at finite time. For a special case as shown in Fig. S3 in Supporting Material where the polygon forms an equilateral triangle between three junction points linking to three persistent points also in equilateral triangle, one can check that Eq. 3 implies that $A(t)$ collapses quadratically to zero. However as illustrated in Fig. 3(a) typical small polygons are asymmetric and collapse linearly to zero.

Quantifying the cross-connection processes

Experimental data shows that new tubules are occasionally and rapidly drawn out of the ER to form links to other tubules. We refer to this as the "cross-connection" process P2: examples are visible in Fig. 1 and Fig. 5. As the process P2 adds new links to the network, it increases the network length, the number of polygons and the number of junction points.

The cross-connections appear to be homogeneously distributed in space and time and thus it makes sense to talk about a rate of cross-connections per unit area that scales linearly with the area of the space in observation. From a number of experimental ER movies, we measure the rate of cross-connections per unit area $\alpha = 0.0048 \pm 0.00085$ ($n = 20$) in units of $s^{-1}\mu m^{-2}$ by manually quantifying the number of observed cross-connection events as described in Methods.

Note that the experiments in [2] with the addition of LatB which depolymerizes the actin, such cross connections rarely occurs. Note also the ER network dynamics are largely driven

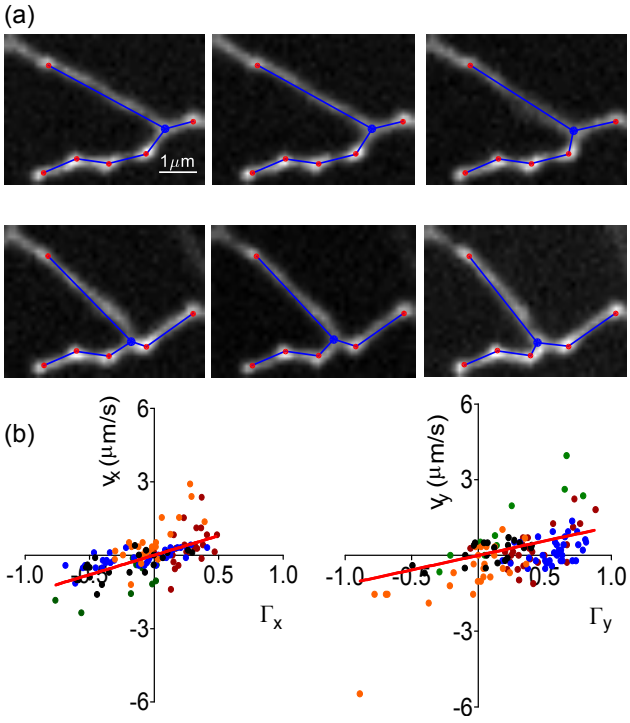

Figure 4: (a) Frames from Movie S4 showing an ER junction point that moves past a sequence of persistent points, remodelling the network in doing so. Frames are overlaid with abstracted networks where red dots indicate persistent points, blue dots indicate the ER junction points and lines represent ER tubules. (b) The force-velocity relation for the ER junction points in both horizontal (left panel) and vertical (right panel) components from 5 experimental data sets including (a) (shown in black dots). The geometric resultant force (Γ_x, Γ_y) is inferred from the geometry of the links to the ER junction point and the velocity (v_x, v_y) is estimated from positions in the movie. Red lines indicate best linear fits through origin with best fitting slope 1.6 (95% confidence interval: $1.21-1.98$) and 1.15 (95% confidence interval: $0.84-1.49$) for the horizontal and vertical components respectively; an F test shows there is no significant difference ($p = 0.109$) in the slope between two vertical and horizontal components. Some outliers may be due to presence of organelles or other forces not visible from the images.

by acto-myosin dependent processes [10]. We therefore expect the process P2 to be associated with actin-based processes (such as actin polymerisation and depolymerisation, and actin-based transport). We do not attempt however to determine the biophysical processes that cause the cross-connections. New ER tubules and cross-connections also presumably appear in streaming regions. However, in this paper we do not attempt to identify cross-connections within streaming, as the rapid evolution within cytoplasmic streams makes it hard to distinguish individual events.

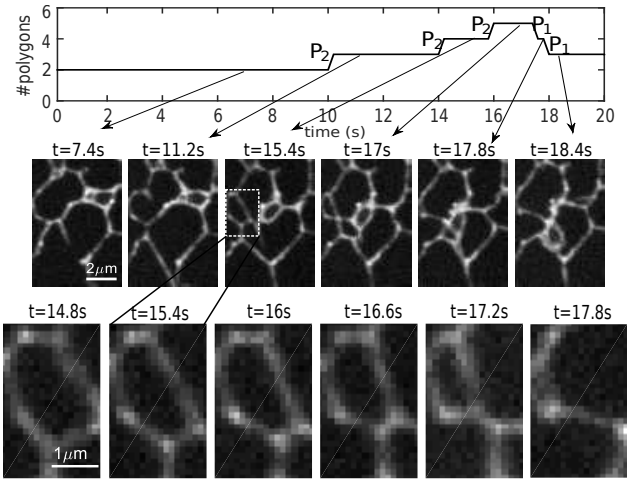

Figure 5: Time series (top pannel) showing dynamics of polygon number during the ER network remodelling. Examples of the ER images at different time points are shown in the middle row, illustrating the "cross-connection" process P2 (which increases the polygon number) and "relaxation" process P1 (which reduces the polygon number). The bottom time series of images show a detailed process of polygon destruction in the highlighted rectangular region.

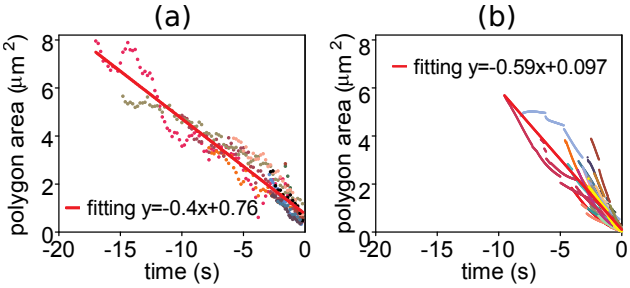

Figure 6: (a) Polygon areas extracted from experimental ER movies ($n = 11$) showing examples of polygons that collapse near $t = 0$. (b) Polygon areas for simulations of the integrative model ($n = 30$) using $b = 1\mu m s^{-1}$. The straight bold red line in each panel gives the best fitting line. Note that polygons shrink at a similar rate in a finite time between experimental data and model simulations. The time axis is translated for visualization effect. We remark here that Brownian fluctuation which appears in experimental data is not included in model simulation.

Validating the integrative model of ER network dynamics

With the quantification of "relaxation" process P1 and "cross-connection" process P2 from image analysis in previous sections, we develop an integrative model (see Methods section) of the two processes. This extends the biophysical model to include the "cross-connection" process that generates new tubules and allows to explore dynamical changes of network morphological. For simplicity, we ignore the Brownian fluctuation (i.e. $\sigma = 0$ in Eq. 2 in

"relaxation" process P1).

We first test if network quantities in equilibrium state are independent of initial states in the dynamics model. With a given set of persistent points, we initialize networks from either (a) a minimal spanning tree or (b) a Delaunay triangulation between the set of persistent points (see Fig. S4 in Supporting Material). After an initial transient, we show in Fig. 7(a) that the network dynamics settles into the same statistically stationary behaviour for both average and maximal network length among simulations. Fig. S5 in Supporting Material shows an example of time series of various network quantities from the model, and illustrates how the number of junction points and maximal speed of junction points increase once a new link is created, and how the network relaxes back towards an ESN configuration until the next cross connection is added: the network is close to ESNs when the maximal speed among junction points is close to zero. Fig. 7(a) and Fig. S5 also demonstrates that the network length oscillates between a wide range of ESNs connecting the same set of persistent points.

Next, we validate our dynamical model in the following ways. As in the experiment, we observe that small polygons usually collapse in finite time from the model simulations. Fig. 6(b) shows some collapsing polygons in the model and finds good quantitative similarity in the profiles of the collapsing polygons: there is a comparable linear collapse rate to that observed in experiments shown in Fig. 6 (a). In addition, using an experimentally measured initial network, persistent points and cross-connection events, the integrative model can reproduce detailed dynamical behaviour; see Fig. 8 (and Movie S5 in Supporting Material). Propagating the junction points leads to dynamic rearrangements of the network in the integrative model that closely parallel those seen in the experimental data.

ER network properties from the integrative model

This integrative model allows exploration of how the network behaviour depends on parameters. Fig. 7(b) shows averages of various network quantities as a function of the cross-connection rate α and effective drift coefficient b for a given set of persistent nodes. Since the model is invariant under an identical scaling of α and b and time, these averaged quantities depend only on the ratio α/b. This can be viewed as a "temperature" of the network perturbations caused by cross connections: larger α/b leads to a more complex transient graphs with more polygons per unit area, more points per unit area, and a longer mean network length per unit area at statistical equilibrium.

We estimate the mean node density ρ (i.e. the number of points per unit area) in the dynamic network given the ratio α/b, at least for small values of this quantity in a heuristic way. For a given density ρ_p of persistent points, the node density increases as cross-connection links are generated and decreases as polygons collapse and their vertices merge. At statistical equilibrium these rates will balance. Let ρ_0 be the average node density with density ρ_p of persistent points at the limit $\alpha/b \to 0$; note that $\rho_0 - \rho_p > 0$ is the (fixed) density of junction points for the ESNs. The rate of increase of node density is twice the cross-connection rate, i.e. 2α, as each new link generates two additional junction points. The rate of decrease of node density, as noted from Fig. 6, is associated with polygon collapse. This occurs at a rate given by the effective drift coefficient b divided by the mean diameter c of a collapsing

polygon, times the excess density of polygons. If we assume that on average m vertices are lost when a polygon collapses and this is constant then the excess density of polygons is $\frac{1}{m}(\rho - \rho_0)$ but we also lose m points at collapse, and so

$$\frac{d\rho}{dt} = 2\alpha - \frac{b}{c}(\rho - \rho_0) \tag{4}$$

After transients have decayed, this gives linear dependence in the mean node density

$$\rho(\alpha, b) = \rho_0 + 2c\frac{\alpha}{b} \tag{5}$$

where ρ_0 and c can be fitted. Fig. 7(b) shows a good fit to Eq. 5 at least for small α/b. This predicts that for higher cross-connection rate or slower effective drift the mean polygon area will be smaller, a prediction confirmed by simulations in Fig. 7(b).

DISCUSSION

Spinning disc confocal imaging of live cell ER is a powerful tool for investigation of many processes involved in the dynamic maintenance of an ER network. Conversely, the integrative model allows us to understand emergent organization of the ER network (such as polygon collapse) and to see how the network dynamics is dependent on parameters. Using only the "relaxation" process P1 and "cross-connection" process P2 we give insight into maintenance of ER dynamics, though even in this case we highlight that large number of local minimum apparently present even for a moderately small number of persistent points. Although we have predicted some of mean network quantities such as node density from Eq. 5, it will be a challenge to quantify the variety of topologies and the ESNs that are approached under the action of P1 and P2. Also, Fig. 7 and Eq. 5 predict that either faster cross connection or slower tension drift will give statistically smaller polygons. In principle, this prediction can be experimentally tested by analysis of the ER when manipulating molecular factors that control ER geometry and dynamics [2, 8, 9, 29, 30, 31, 32, 33, 34, 35, 36].

A more sophisticated model will take other biophysical processes into account. One such process is the Brownian force included in Eq. 2: Movie S6 in Supporting Material shows the network dynamics including Brownian fluctuation with the estimated diffusion rate $\sigma = 0.002\mu m^2\, s^{-1}$. A higher diffusion rate can enhance "cross-connection" process and the network dynamics and generate more polygons. However a more efficient algorithm and possibly resolution of tubule curvature will be needed to accurately model the effects of Brownian motion on network remodelling. Other processes include organelle interactions with ER [4], cytoplasmic streaming (as shown in Fig. 1), "pinning/unpinning" of the network to persistent points in the plasma membrane (as suggested in [23]). Of these, pinning/unpinning places/removes constraints on the networks and any rearrangements thereof; this is generally observable in conjunction with streaming and otherwise seems to occur very rarely. Streaming remains the most difficult process to quantify as it occurs on fast time scales that are hard to resolve, and it appears to randomly rotate and reorient within the cortex. Better temporal and spatial resolutions of ER microscopy may help to resolve these processes.

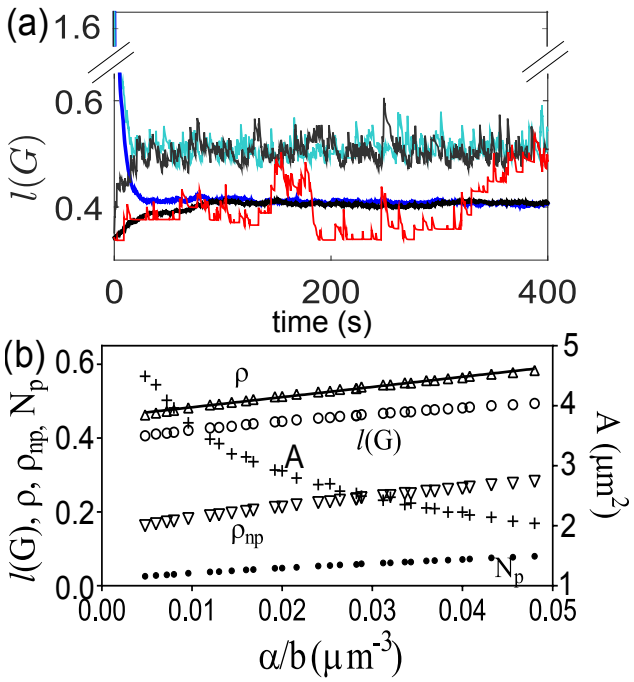

Figure 7: (a) Network length $l(G)$ per unit area from a simulation of the integrative model with $\alpha = 0.0048 s^{-1}\mu m^{-2}$ and $b = 1\mu m\, s^{-1}$ for a set of 30 uniformly distributed persistent points in a $10\mu m \times 10\mu m$ region, starting at two different initial topologies. Black/grey (resp. blue/light blue) curves show averages/maxima over 100 simulation starting with a minimal spanning tree (resp. Delaunay triangulation). The red curve shows a typical realization starting at a minimal spanning tree. There is a rapid transient decay to a statistically stationary state. (b) Averages of network quantities as a function of α/b from the integrative model with the same set of persistent points as in (a). Quantities include network length per unit area $l(G)$ ($\circ$, μm^{-1}), density of junction points (non-persistent points) ρ_{np} and all points (ρ) per unit area ($\bigtriangledown$, $\bigtriangleup$ respectively, μm^{-2}), no. of polygons N_p per unit area ($\cdot$, μm^{-2}) and mean polygon area A ($+$, μm^2). The best fit of ρ to Eq. 5 has parameters $\rho_0 = 0.456 \mu m^{-2}$, $c = 1.37\ \mu m$. Each quantity is averaged over $500 - 2000 s$ and 100 simulations.

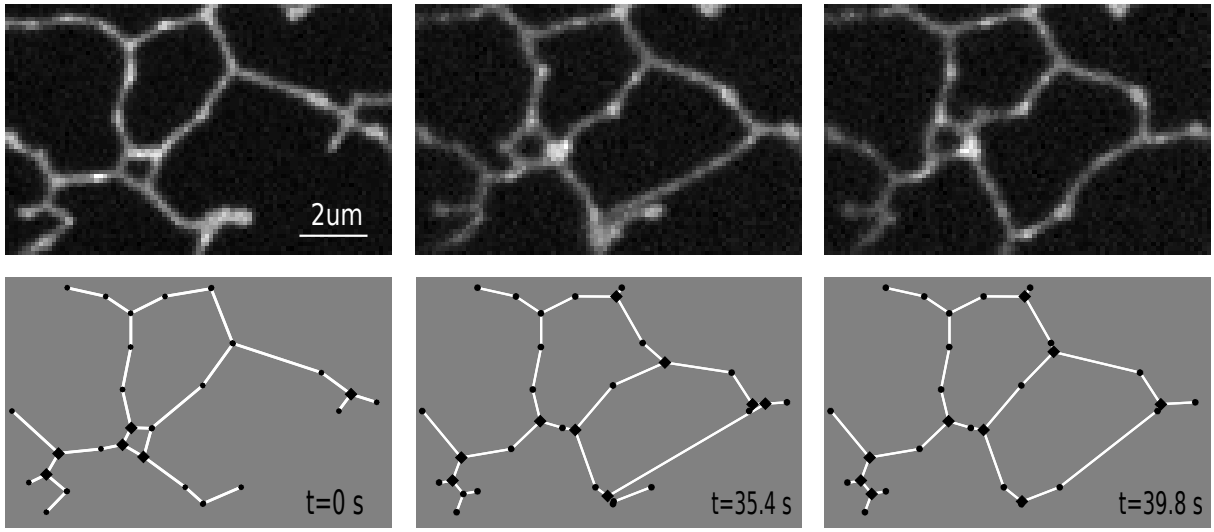

Figure 8: Example of ER network dynamics in the experiment (top panels) and the model (bottom panels). Black dots in the lower panels are persistent points extracted from the experimental ER movie while black squares are junction points in the model. We use an estimated effective drift coefficient $b = 1\mu m\, s^{-1}$. One cross connection is created at $t = 35.4s$, comparable to that in the experiment. After a few seconds, the network configuration in the model reaches a steady state which is similar to observed ER network in experiments (right two panels). The small mobile polygon in the experiments is probably due to the ER wrapping around an organelle (not included in the model). See Movie S5 in Supporting Material for a comparison between model and experimental data during the evolution.

For a more detailed model of ER structural dynamics, one will need to model not only ER tubules as filaments whose tension is determined by the ER membrane surface tension but also ER sheets, more complex (e.g. helicoidal) structures as well as viscoelastic properties of the ER membrane. Bending and curvature of ER membrane in 3D will occur when tubules link or are drawn out during ER dynamics. We note that when ER junction points move rapidly through stationary cytoplasm, ER tubules can be observed to be transiently curved as a result of viscous drag along the tubule filament (slight bending can be observed in some tubules of Fig. 4). In terms of viewing ER as an optimal structure for system energy, instead of simply minimizing the ER membrane surface energy (subject to constraints of persistent anchoring points), a more realistic model will need to take into account other contributions to system energy (e.g. bending energy [15, 16]). Modelling the dynamics of such more realistic structures in future will help to build a more complete model and understand more of the critical biophysical process in play for ER dynamics.

SUPPORTING MATERIAL

Supporting Material includes detailed descriptions of the mean square displacement analysis and the model simulation of network dynamics, 5 supporting figures and 6 supporting movies.

AUTHOR CONTRIBUTION

P.A. and I. S. developed the research plan and directed the project. C.L. and P.A. developed the model and wrote the manuscript (with exception of Experimental Methods, which were written by R.R.W). C.L. analysed the data. R.R.W. prepared the samples and operated the spinning disc microscope. All authors corrected the manuscript and discussed data.

ACKNOWLEDGEMENTS

This work was funded by a Leverhulme Trust grant (RPG-2015-106). We would like to thank Laurent Lemarchand for his helpful suggestions on polygon computation from the model.

References

[1] Puhka, M., H. Vihinen, M. Joensuu, and E. Jokitalo. 2007. Endoplasmic reticulum remains continuous and undergoes sheet-to-tubule transformation during cell division in mammalian cells. *J. Cell Biol.* 179:895-909.

[2] Sparkes, I. A., J. Runions, C. Hawes, and L. Griffing. 2009. Movement and Remodeling of the Endoplasmic Reticulum in Nondividing Cells of Tobacco Leaves. *Plant Cell* 21:3937-3949.

[3] Sparkes, I., C. Hawes, and L. Frigerio. 2011. FrontiERs: movers and shapers of the higher plant cortical endoplasmic reticulum. *Curr. Opin. Plant Biol.* 14:658-665.

[4] Sparkes, I. A., T. Ketelaar, N.C. de Ruijter, and C. Hawes. 2009. Grab a Golgi: laser trapping of Golgi bodies reveals in vivo interactions with the endoplasmic reticulum. *Traffic* 10:567-71.

[5] Friedman, J. R., and G. K. Voeltz. 2011. The ER in 3D: a multifunctional dynamic membrane network. *Trends in Cell Biology* 21:709-717.

[6] Jaipargas E., K.A. Barton, N. Mathur and J. Mathur. 2015. Mitochondrial pleomorphy in plant cells is driven by contiguous ER dynamics. *Frontiers in plant science* 6:783.

[7] Schattat M., K. Barton, B. Baudisch, R.B. Klsgen, J. Mathur. 2011. Plastid stromule branching coincides with contiguous endoplasmic reticulum dynamics. *Plant Physiol.* 155:1667-1677.

[8] Ueda, H., E. Yokota, N. Kutsuna, T. Shimada, K. Tamura, T. Shimmen, S. Hasezawa, V. V. Dolja, and I. Hara-Nishimura. 2010. Myosin-dependent endoplasmic reticulum motility and F-actin organization in plant cells. *Proc. Natl. Acad. Sci. U.S.A.* 107:6894-6899.

[9] Goyal, U., and C. Blackstone. 2013. Untangling the web: Mechanisms underlying ER network formation *Biochim Biophys Acta.* 1833:2492-2498.

[10] Hamada, T., H. Ueda, T. Kawase, I. Hara-Nishimura. 2014. Microtubules contribute to tubule elongation and anchoring of endoplasmic reticulum, resulting in high network complexity in Arabidopsis. *Plant Physiol.* 166:1869-1876.

[11] Radochová, B., J. Janáček, K. Schwarzerová, E. Demjénová, and Z. Torori. 2005. Analysis of endoplasmic reticulum of tobacco cells using confocal microscopy. *Image Anal. Stereol.* 24:181-185.

[12] Puhka, M., M. Joensuu, H. Vihinen, I. Belevich, and E. Jokitalo. 2012. Progressive sheet-to-tubule transformation is a general mechanism for endoplasmic reticulum partitioning in dividing mammalian cells. *Mol. Biol. Cell* 23: 2424-2432.

[13] West, M., N. Zurek, A. Hoenger, and Gia K. Voeltz. 2011. A 3D analysis of yeast ER structure reveals how ER domains are organized by membrane curvature. *J. Cell Biol.* 193:333-346.

[14] Bouchekhima, A. N., L. Frigerio, and M. Kirkilionis. 2009. Geometric quantification of the plant endoplasmic reticulum. *J. of Microscopy* 234:158-172.

[15] Terasaki, M., T. Shemesh, N. Kasthuri, .W. Klemm, R. Schalek, K.J. Hayworth, A.R. Hand, M. Yankova, G. Huber, J.W. Lichtman, T.A. Rapoport, and M.M. Kozlov. 2013. Stacked endoplasmic reticulum sheets are connected by helicoidal membrane motifs. *Cell* 154:285-296.

[16] Shemesha, T., R.W. Klemm, F.B. Romano, S. Wang, J. Vaughan, X. Zhuang, H. Tukachinsky, M.M. Kozlove and T.A. Rapoport. 2014. A model for the generation and interconversion of ER morphologies. *Proc. Natl. Acad. Sci. U.S.A.* 111:E5243-E5251.

[17] Sparkes, I., L. Frigerio, N. Tolley, and C. Hawes. 2009. The plant endoplasmic reticulum: a cell-wide web. *Biochem. J.* 423:145-155.

[18] Griffing, L. R. 2010. Networking in the endoplasmic reticulum. *Biochem. Soc. Trans.* 38:747-753.

[19] Wang, P., T.J. Hawkins, C. Richardson, I. Cummins, M.J. Deeks, I. Sparkes, C. Hawes, P.J. Hussey. 2014. The plant cytoskeleton, NET3C, and VAP27 mediate the link between the plasma membrane and endoplasmic reticulum. *Curr Biol.* 24:1397-405.

[20] Levy, A., J.Y. Zheng, S.G. Lazarowitz. 2015. Synaptotagmin SYTA forms ER-plasma membrane junctions that are recruited to plasmodesmata for plant virus movement. *Curr. Biol.* 25:2018-2025.

[21] Prez-Sancho, J., S. Vanneste, E. Lee, H.E. McFarlane, A. Esteban Del Valle, V. Valpuesta, J. Friml, M.A. Botella, A. Rosado. 2015. The Arabidopsis synaptotagmin1 is enriched in endoplasmic reticulum-plasma membrane contact sites and confers cellular resistance to mechanical stresses. *Plant Physiol.* 168:132-143.

[22] Siao, W., P. Wang, B. Voigt, P.J. Hussey, F. Baluska. 2016. Arabidopsis SYT1 maintains stability of cortical endoplasmic reticulum networks and VAP27-1-enriched endoplasmic reticulum-plasma membrane contact sites. *J. Exp. Bot.* 67:6161-6171.

[23] Lin, C., Y. Zhang, I. Sparkes, P. Ashwin. 2014. Structure and dynamics of ER: minimal networks and biophysical constraints. *Biophys J* 107:763-772.

[24] Hwang, F. K., D. S. Richards, and P. Winter. The Steiner tree problem. *Annals of Discrete Mathematics*. Vol. 53. Elsevier Science Publishers B.V., North-Holland, Amsterdam (1992).

[25] Sparkes, I., J. Runions, A. Kearns and C. Hawes. 2006. Rapid, transient expression of fluorescent fusion proteins in tobacco plants and generation of stably transformed plants. *Nat. Protoc.* 1:2019-2025.

[26] Nelson B.K., X. Cai and A. Nebenführ. 2007. A multicolored set of in vivo organelle markers for co-localization studies in Arabidopsis and other plants. *Plant J.* 51:1126-136.

[27] Coffey, W. T., and Y. P. Kalmykov. The Langevin Equation: With Applications to Stochastic Problems in Physics, Chemistry and Electrical Engineering (Third edition), World Scientific Series in Contemporary Chemical Physics - Vol 14.

[28] Perry, George L.W., Ben P. Miller and Neal J. Enright. 2006. A comparison of methods for the statistical analysis of spatial point patterns in plant ecology. *Plant Ecology* 187:59-82.

[29] Griffing, L., H. T. Gao, and I. Sparkes. 2014. ER network dynamics are differentially controlled by myosins XI-K, XI-C, XI-E, XI-I, XI-1 and XI-2. *Front. Plant Sci.* 5:218.

[30] Griffing, L.R., C. Lin, C. Perico, R.R. White, and I. Sparkes. Plant ER geometry and dynamics: biophysical and cytoskeletal control during growth and biotic response. 254:43-56.

[31] Tolley, N., I. Sparkes, P.R. Hunter, C.P. Craddock, J. Nuttall, L.M. Roberts, C. Hawes, E. Pedrazzini, L. Frigerio. 2008. Overexpression of a plant reticulon remodels the lumen of the cortical endoplasmic reticulum but does not perturb protein transport. *Traffic* 9:94-102.

[32] Sparkes, I., N. Tolley, I. Aller, J. Svozil, A. Osterrieder, S. Botchway, C. Mueller, L. Frigerio, C. Hawes. 2010. Five Arabidopsis reticulon isoforms share endoplasmic reticulum location, topology, and membrane-shaping properties. *Plant Cell.* 22:1333-1343.

[33] Tolley, N., I. Sparkes, C.P. Craddock, P.J. Eastmond, J. Runions, C. Hawes, L. Frigerio. 2010 Transmembrane domain length is responsible for the ability of a plant reticulon to shape endoplasmic reticulum tubules in vivo. *Plant J.* 64:411-418.

[34] Lee, H., I. Sparkes, S. Gattolin, N. Dzimitrowicz, L.M. Roberts, C. Hawes, L. Frigerio. 2013. An Arabidopsis reticulon and the atlastin homologue RHD3-like2 act together in shaping the tubular endoplasmic reticulum. *New Phytol.* 197:481-489.

[35] Ueda, H., E. Yokota, K. Kuwata, N. Kutsuna, S. Mano, T. Shimada, K. Tamura, G. Stefano, Y. Fukao, F. Brandizzi, T. Shimmen, M. Nishimura, I. Hara-Nishimura. 2016. Phosphorylation of the C Terminus of RHD3 Has a Critical Role in Homotypic ER Membrane Fusion in Arabidopsis. *Plant Physiol.* 170:867-880.

[36] Breeze, E., N. Dzimitrowicz, V. Kriechbaumer, R. Brooks, S.W. Botchway, J.P. Brady, C. Hawes, A.M. Dixon, J.R. Schnell, M.D. Fricker, L. Frigerio. 2016. A C-terminal amphipathic helix is necessary for the in vivo tubule-shaping function of a plant reticulon. *Proc. Natl. Acad. Sci. U.S.A.* 113:10902-10907.